Quantifying the effect of electric current on cell adhesion studied by single-cell force spectroscopy

Jaatinen, Leena ; Young, Eleanore ; Hyttinen, Jari ; Vörös, János ; Zambelli, Tomaso ; Demkó, László

Abstract: This study presents the effect of external electric current on the cell adhesive and mechanical properties of the C2C12 mouse myoblast cell line. Changes in cell morphology, viability, cytoskeleton, and focal adhesion structure were studied by standard staining protocols, while single-cell force spectroscopy based on the fluidic force microscopy technology provided a rapid, serial quantification and detailed analysis of cell adhesion and its dynamics. The setup allowed measurements of adhesion forces up to the N range, and total detachment distances over 40 m. Force–distance curves have been fitted with a simple elastic model including a cell detachment protocol in order to estimate the Young's modulus of the cells, as well as to reveal changes in the dynamic properties as functions of the applied current dose. While the cell spreading area decreased monotonously with increasing current doses, small current doses resulted only in differences related to cellelasticity.Current doses above 11 As/m2, however, initiated more drastic changes in cell morphology, viability, cellular structure, as well as in properties related to cell adhesion. The observed differences, eventually leading to cell death toward higher doses, might originate from both the decrease in pH and the generation of reactive oxygen species.

DOI: https://doi.org/10.1116/1.4940214

Originally published at:
Jaatinen, Leena; Young, Eleanore; Hyttinen, Jari; Vörös, János; Zambelli, Tomaso; Demkó, László (2016). Quantifying the effect of electric current on cell adhesion studied by single-cell force spectroscopy. Biointerphases, 11(1):011004.
DOI: https://doi.org/10.1116/1.4940214

Biointerphases
A Journal of Biomaterials and Biological Interfaces

Quantifying the effect of electric current on cell adhesion studied by single-cell force spectroscopy

Leena Jaatinen, Eleanore Young, Jari Hyttinen, János Vörös, Tomaso Zambelli, and László Demkó

Citation: Biointerphases **11**, 011004 (2016); doi: 10.1116/1.4940214
View online: http://dx.doi.org/10.1116/1.4940214
View Table of Contents: http://scitation.aip.org/content/avs/journal/bip/11/1?ver=pdfcov
Published by the AVS: Science & Technology of Materials, Interfaces, and Processing

Quantifying the effect of electric current on cell adhesion studied by single-cell force spectroscopy

Leena Jaatinen
Laboratory of Biosensors and Bioelectronics, Institute for Biomedical Engineering, ETH Zurich, CH-8092 Zurich, Switzerland and Department of Electronics and Communications Engineering, Tampere University of Technology, BioMediTech, Finn-Medi 1 L 4, Biokatu 6, FI-33520 Tampere, Finland

Eleanore Young
Laboratory of Biosensors and Bioelectronics, Institute for Biomedical Engineering, ETH Zurich, CH-8092 Zurich, Switzerland

Jari Hyttinen
Department of Electronics and Communications Engineering, Tampere University of Technology, BioMediTech, Finn-Medi 1 L 4, Biokatu 6, FI-33520 Tampere, Finland

János Vörös, Tomaso Zambelli, and László Demkó[a)]
Laboratory of Biosensors and Bioelectronics, Institute for Biomedical Engineering, ETH Zurich, CH-8092 Zurich, Switzerland

(Received 2 November 2015; accepted 7 January 2016; published 20 January 2016)

This study presents the effect of external electric current on the cell adhesive and mechanical properties of the C2C12 mouse myoblast cell line. Changes in cell morphology, viability, cytoskeleton, and focal adhesion structure were studied by standard staining protocols, while single-cell force spectroscopy based on the fluidic force microscopy technology provided a rapid, serial quantification and detailed analysis of cell adhesion and its dynamics. The setup allowed measurements of adhesion forces up to the μN range, and total detachment distances over 40 μm. Force–distance curves have been fitted with a simple elastic model including a cell detachment protocol in order to estimate the Young's modulus of the cells, as well as to reveal changes in the dynamic properties as functions of the applied current dose. While the cell spreading area decreased monotonously with increasing current doses, small current doses resulted only in differences related to cell elasticity. Current doses above 11 As/m^2, however, initiated more drastic changes in cell morphology, viability, cellular structure, as well as in properties related to cell adhesion. The observed differences, eventually leading to cell death toward higher doses, might originate from both the decrease in *p*H and the generation of reactive oxygen species. © *2016 American Vacuum Society*. [http://dx.doi.org/10.1116/1.4940214]

I. INTRODUCTION

Cells adapt to their environment and external stimuli predominantly by altering their mechanical properties, which have shown to be correlated with cell structure and function.[1–3] Electric stimulus, in particular, can influence cell properties and functions such as adhesion, the arrangement of the cytoskeleton, proliferation, growth factor and gene expression, and cell viability.[4–6] At the subcellular level, electric stimulation of mammalian cells induces different physiological responses including changes in calcium dynamics[7,8] and the redistribution of surface receptors.[9,10] The inhibition of linker protein binding and increase in growth factor binding to the redistributed surface receptors result in actin cytoskeleton reorganization and membrane–cytoskeleton dissociation, and ultimately lead to alterations in the cell morphology and cytoskeleton elasticity.[2,8,11] Cell morphology is closely related to cell adhesion, which plays a crucial role in cell survival, migration, differentiation, and tissue organization. Cells adhere to the extracellular matrix predominantly via transmembrane cell adhesion proteins, such as integrins. Integrins bind to the cytoskeleton via adapter proteins like vinculin and paxillin,[12] and form large and prominent actin-linked cell–matrix junctions called focal adhesions. Previous studies show that blocking the Ca^{2+} channels inhibits the integrin-mediated cell adhesion, and as such, electric stimulus modifies the cell adhesion also via changing the calcium dynamics.[13,14]

The effect of electric current on cells depends on the stimulation parameters such as the polarity, magnitude, and stimulation time.[6] In addition, results found in the literature are often seemingly contradictory, especially in terms of cell adhesion and migration, because electricity affects the electrocoupling mechanisms and specific signaling pathways differently depending on the cell type and culturing conditions, and thus, cell responses show a high variability.[8,15,16] For example, direct currents increase stem cell adhesion to collagen gels,[4] whereas fibroblasts and bone marrow osteoprogenitor cells exposed to direct or low-frequency alternating currents results in cell detachment from culture plates.[17] Steady direct electric currents, depending on the polarity, can generate toxic compounds in a direct electrochemical

[a)]Electronic mail: demko@biomed.ee.ethz.ch

way, or via damaging the electrodes. This effect can be reduced or completely avoided by using alternating currents[18] or pulsed direct currents.[19,20] Constant electric fields cannot penetrate the cell membrane due to its high resistance, but they can trigger molecular signaling pathways at the cell surface by activating voltage-gated calcium channels, plasma membrane receptors, or stretch-activated cation channels.[2] Electric current also changes the local *p*H in the close vicinity of the electrode due to water electrolysis, which affects the stability of protein layers at the electrode and modifies the cell adhesion properties.[21] However, cell-type variability is important here as well. Melanoma cells, for example, adhere stronger when cultured in acidic extracellular *p*H,[22] and also fibroblasts show stronger adhesion on acid-containing hydrogels.[23] Isolated focal adhesions have demonstrated to be the most stable at *p*H below 6 and above 7.2, and unstable between *p*H 6.4 and 6.8.[24]

Traditionally, cell adhesion was studied with indirect, qualitative methods such as hydrodynamic assays where cells were washed off from the surface by shear stress in a rather uncontrolled fashion, or the adhesion strength has been estimated by analyzing the cell morphology and the size and number of focal adhesions.[25,26] Recent efforts generated a significant progress in developing quantitative methods for the direct measurement of single-cell adhesion forces[27] with the help of micropipettes,[28] magnetic[29] and optical[30] tweezers, as well as atomic force microscopy (AFM).[31–33] One of the latest advances include fluidic force microscopy (FluidFM), the combination of the AFM technology and microfluidics,[34] which made the rapid, serial quantification of adhesion forces possible by the reversible immobilization of cells to the cantilever with the help of an applied negative pressure.[35,36] In this work, we investigated the effect of external electric current on the cell adhesive and mechanical properties of C2C12 mouse myoblast cells. C2C12 is a well-established cell line, used already to quantitatively study the effect of electric current on cell viability,[37] as well as to electrically control cell adhesion, growth, and migration.[38] Apart from the standard staining protocols used to investigate viability and cellular structure, here we present, for the first time, a FluidFM-based method to quantify the changes in cell adhesion forces due to applied external electric currents. In addition to the fast, serial single-cell measurements, we were able to quantify adhesion forces up to the μN range, which is at the moment not possible with any other method. Force–distance curves have been fitted with a simple elastic model including a cell detachment protocol, which made it possible to estimate the Young's modulus of the cells and evaluate it as a function of the applied current dose.

II. MATERIALS AND METHODS

A. Cell culture and experimental setup

Mouse myoblast C2C12 cells (American type cell collection) were used in all the experiments. Cells were cultured in Dulbecco's modified eagle medium, nutrient mixture F-12 supplemented with 10% fetal bovine serum and 1% antibiotic-antimycotic (all from Thermo Fisher Scientific AG, Switzerland). The electrical stimulation setups consisted of indium tin oxide (ITO) coated glass slides (MicroVacuum, Ltd., Hungary) mounted into custom-made chambers of poly(methyl methacrylate) base and polytetrafluoroethylene housing. Two different types of chambers and ITO electrodes were used for the experiments, see supplementary material S1 for the details of the different configurations.[39] Chambers were cleaned for 10 min in 70% ethanol, rinsed with Milli-Q water, then left in a laminar flow hood to dry until the ITO was cleaned in 2% sodium dodecyl sulfate for 20 min and rinsed with Milli-Q water, followed by blow drying with nitrogen gas and 2 min plasma cleaning in oxygen atmosphere. Prior to the experiments, chambers were incubated with cell culture medium for 20 min, followed by seeding of 60 000 and 20 000 cells/cm^2 in the small and big chambers, respectively. Cells were incubated for at least 2 h before the electrical stimulation was started. All experiments and incubation were carried out at 37 °C in a humidified 5% CO_2 atmosphere if not indicated otherwise.

As external stimuli, anodic, pulsed monophasic currents were applied to the ITO working electrodes using an Autolab PGSTAT 302N potentiostat/galvanostat (Metrohm Autolab B.V., Netherlands). The alternating current on and off periods were both 5 s long, with an applied current density of 0.01 A/m^2, except in the case of studying the effect of different current densities on the total number of live cells at constant current doses, when the current densities of 0.01 and 0.03 A/m^2 have been used. Current doses (As/m^2) were calculated from the total current on time for each current density. The anodic current is expected to lower the *p*H in the close vicinity of the ITO surface, making the fluidic environment around the cells more acidic.[37]

B. Viability and focal adhesion staining

Cell viability was visualized by fluorescent live/dead staining. After applying the stimulation protocol, medium and possibly nonattached cells were removed, and the remaining cells were stained with a mixture of 1 μM calcein AM and 3 μM ethidium homodimer-1 (both from Thermo Fisher Scientific) diluted in 1 ml phosphate-buffered saline (PBS) for live and dead cells, respectively. After 30 min of incubation, the probe solution was replaced with culture medium, and fluorescent images were taken with an inverted microscope (DM IL; Leica Microsystems AG, Switzerland). The viability of the C2C12 cells in control conditions has found to be (99 ± 1)%.

For visualizing focal adhesions, cells were fixed in 4% paraformaldehyde and permeabilized with 0.5% Triton X-100. Background binding was blocked by incubating for 1 h at room temperature in a solution of 3% bovine serum albumin diluted in PBS, followed by overnight incubation with mouse monoclonal antivinculin antibody (1:1000; Sigma-Aldrich Chemie GmbH, Switzerland) at 4 °C. After washing with PBS, samples were incubated at room temperature for 1 h with Cy3-conjugated goat antimouse secondary antibody (1:100), phalloidin (1:500) and DAPI (1:200) (all from Sigma-Aldrich Chemie), for visualizing vinculin, F-

actin, and nucleus, respectively, and imaged with a fluorescence microscope (CTR 6000; Leica Microsystems).

C. Adhesion force measurements

The FluidFM setup for measuring cell adhesion forces has been described in detail previously.[35] In brief, a hollow cantilever with a microfluidic channel (Cytosurge AG, Switzerland) was mounted on an atomic force microscope head (FlexAFM; Nanosurf AG, Switzerland) and placed on an inverted microscope (Axio Observer.Z1; Carl Zeiss AG, Switzerland) above the sample chamber fixed to a z-stage (Nanosurf). The cantilevers used for the present study were rectangular, tipless silicon nitride probes with apertures of 8 μm in diameter connected to a pressure controller (Cytosurge). The size of the aperture was selected to be large enough to apply sufficient force to detach the cells from the substrate without damaging the cell membrane, and also small enough to be able to position it entirely on the adhered cells.

Prior to the experiments, all the cantilevers were calibrated for their spring constants [k (N/m)] based on the theory of Sader *et al.*,[40] and filled with Milli-Q water from the reservoir by applying an overpressure. Since the position of the AFM sensing laser on the cantilever can slightly change between experiments and this affects the measured force signal, the sensitivity of the cantilevers [S (V/nm)] was measured at the beginning of all the experiments by performing force spectroscopy on cell-free areas of the ITO substrate. The sensitivity translates the photo detector signal [V (volts)] to the bending of the cantilever (nm), and the force (F) is derived from $F = k \times V/S$.

During the cell adhesion force measurements, individual cells were approached in contact mode with a set point of 5 nN and a speed of 1 μm/s. Once the cantilever was brought into contact with the cell membrane, a negative pressure of 800 mbar was applied. After 10 s, enough for establishing a stable contact between the probe and the cell, the probe was retracted with the same speed, while the pressure was maintained and the deflection signal of the probe was recorded until the cell had completely detached from the surface. As the last, cleaning step, a positive pressure of 1000 mbar was applied to prevent further adhesion of the cell on and inside the probe. After each adhesion measurement, the measurement chamber was quickly replaced by containers of cleaning solutions without removing the cantilever from the scan head and disconnecting it from the pressure controller. The cantilevers were cleaned by dipping them first in 5% sodium hypochlorite, then thrice in Milli-Q water for a few seconds. After the experiments, cantilevers were stored in Milli-Q water supplemented with 2% antibiotic–antimycotic (Thermo Fisher Scientific). With this cleaning protocol cantilevers could be used for 10–50 measurement cycles typically, unless they got mechanically damaged.

D. Statistics

For assessing cell spreading area and viability, three independent experiments were carried out in every current dose group described later. Cell spreading areas were determined, and live and dead cells were counted at three different locations each, on both the current-applied and control electrodes. For adhesion force measurements, force–distance curves of 43 cells in total were measured, each current dose group consisting of at least five measurements. Sensitivity of the cantilevers during the individual experiments has been calculated as the mean of three sensitivity measurements performed on different areas of the bare ITO substrate. Results are presented as mean $\pm$ standard error, and a non-parametric t-test with the Mann-Whitney test has been used to determine the statistically significant ($p < 0.05$, $p < 0.01$, and $p < 0.001$) differences between control and the different current dose groups.

III. RESULTS AND DISCUSSIONS

A. Cell morphology and viability

As represented in Fig. 1(a), in control conditions with no applied current cells adhered and spread on the ITO electrodes. Following Fig. 2(a), even though the cell area decreases monotonously with increasing current doses, at the early stage of the stimulation, cell morphology did not change and viability showed no decrease for current doses smaller than 11 As/m^2, as shown in Figs. 1(b), 1(c), 2(b), and S2 of the supplementary material. With a drop in viability, at current doses above 11 As/m^2 the live cell population shrank to approximately 50% of the control both in viability and cell area, and the cell morphology started to change from well spread to more rounded shapes [Fig. 1(d)]. Stimulating with current doses higher than 16 As/m^2, the cell morphology became even more rounded, and also alteration in the nucleus were detected [Fig. 1(e)], while above 20 As/m^2 all the cells appeared circular and dead [Figs. 1(f) and S2(f)], with the cell area shrinking below 40% of the control. According to Gabi *et al.*,[37] with increasing current doses the extracellular pH is decreasing remarkably. In our case this effect might have caused the cell death directly,[41] but reactive oxygen species (ROS) generated by the applied current could also catalyze the effect. The amount of ROS released to the medium is proportional to the applied current dose.[42,43] Small amounts of ROS can alter, and usually increase cell adhesion,[44,45] but intermediate concentrations have been associated with the loss of focal adhesions,[46] and high amounts of ROS cause cell death.[47] As demonstrated in Fig. 2(c), at moderate current doses ($\leq$16 As/m^2), cell viability was rather correlated with the current dose (As/m^2) than the current density (A/m^2). However, toward higher current doses, lower current densities applied for longer times were more lethal than higher current densities for shorter times, possibly due to the accumulation of ROS.

B. Changes in the cytoskeleton and focal adhesion

In order to find out if stimulation with electric current caused changes in the focal adhesion sites or in the cytoskeleton itself, cells were stained against vinculin what is one of the most prominent parts of focal adhesion complex, and

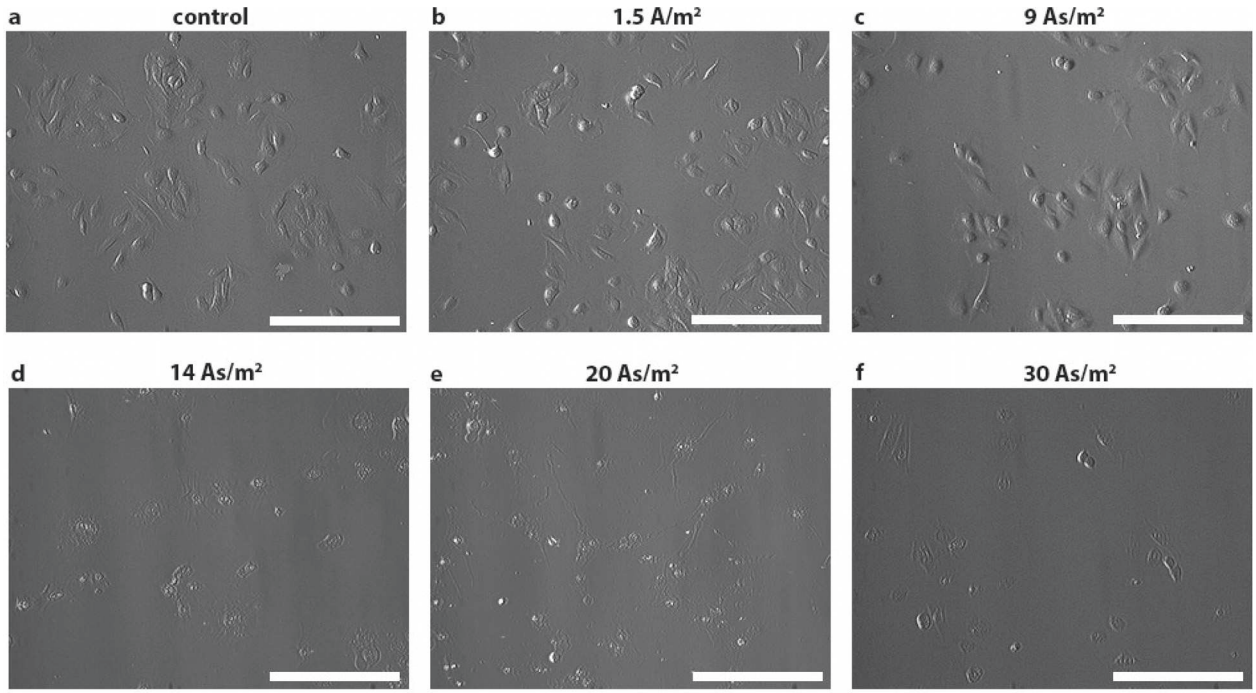

FIG. 1. Cell morphology in control conditions and after being exposed to different current doses. Only current doses above 11 As/m^2 had visible effects on the cell morphology. Scale bars are 200 μm.

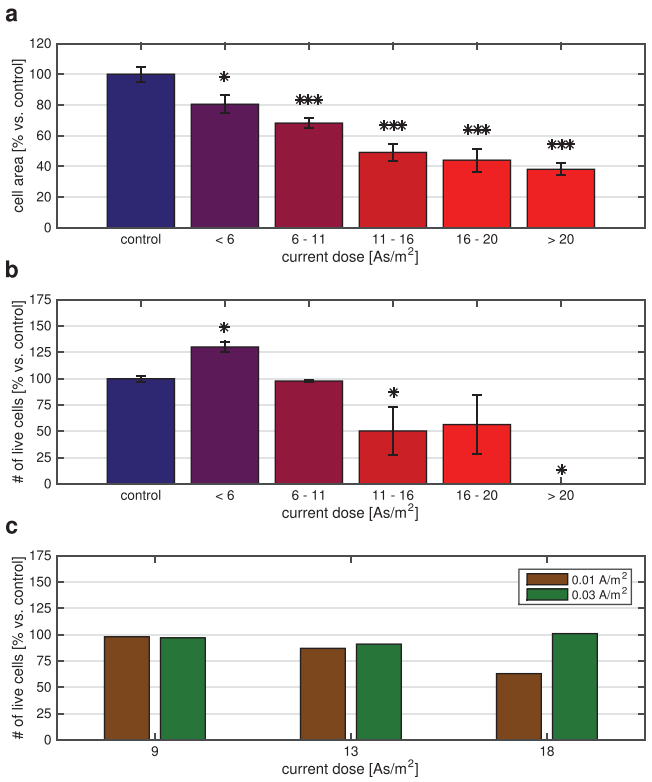

FIG. 2. (a) Cell spreading area at different current doses as compared to the control. (b) Number of live cells on a unit surface at different current doses as compared to the control. At current doses higher than 20 As/m^2, all cells were dead. (c) The effect of different current densities on the total number of live cells at constant current doses. In panels (a) and (b), data are presented as mean $\pm$ the standard error, while single and triple asterisks indicate $p < 0.05$ and $p < 0.001$ significance levels as compared to the control, respectively.

F-actin, the filamentous structures found in cytoskeleton. It is known that vinculin is important for adhesive strength. Increasing the external or internal forces acting on the cell results in the assembly of focal adhesions, while a decrease in the forces results in disassembled or shrunk focal adhesions.[48] Following the fluorescent images of Fig. 3, in control conditions and current doses up to 15 As/m^2, actin fibers were clearly visible, and vinculin was aggregated into focal adhesions at the ends of the actin fibers [Figs. 3(a)–3(d)]. As the current dose reached 15 As/m^2 and cell morphology started to become more rounded, less clear actin fibers and vinculin structures were seen [Fig. 3(e)], while at even higher current doses when cell morphology became circular, also the vinculin structures had disassembled [Fig. 3(f)]. See Figs. S3 and S4 of the supplementary material for representative images of the individual channels corresponding to vinculin and phalloidin (F-actin), respectively.

C. Adhesion force measurements

Alterations in cell morphology and viability can be traced also indirectly, through adhesion force measurements, which also reveal properties of the cytoskeleton and focal adhesions. For this, with the help of the applied negative pressure, individual C2C12 cells were reversibly attached to the cantilever and were detached from the ITO substrate by retracting the cantilever, while the corresponding force–distance curves were recorded. The top and side views of Fig. 4, the latter inspired by Gonnermann *et al.*,[49] as well as the supplementary movies M1–M5 demonstrate the process. See supplementary material S2 for the details on how to use a miniature

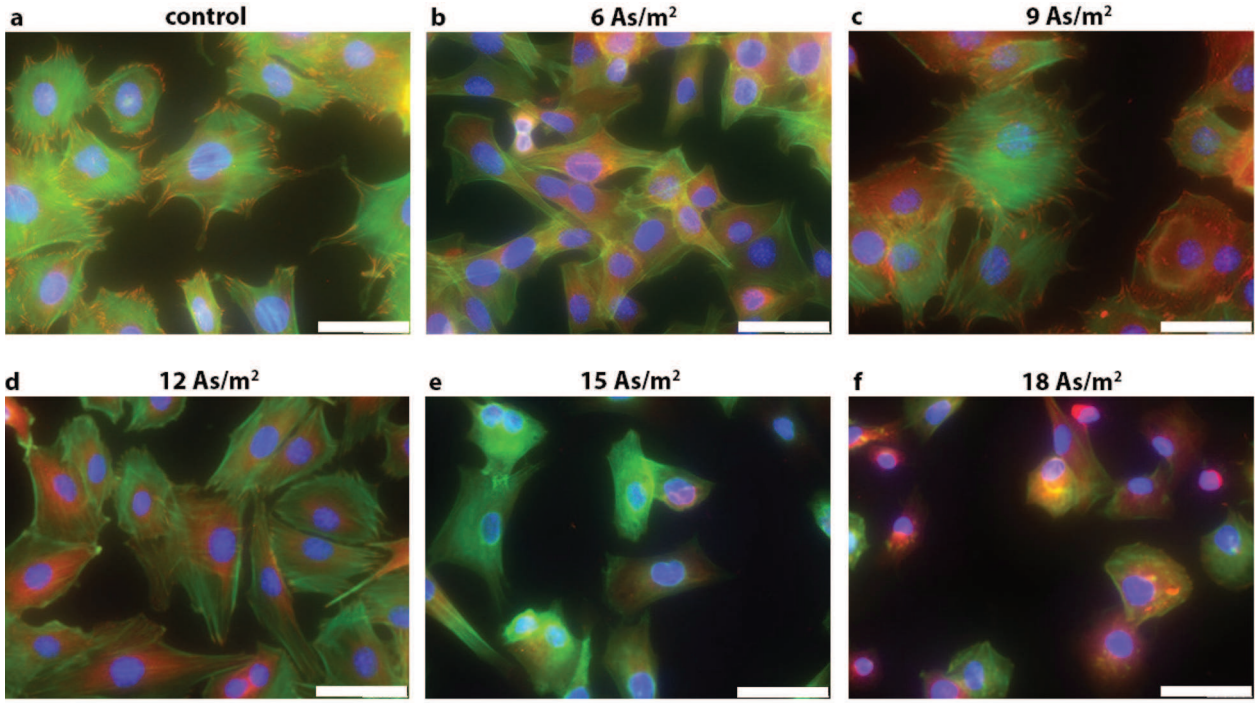

FIG. 3. Fluorescent images of C2C12 cells in control conditions and after stimulated with different current doses, stained with vinculin (red), phalloidin (for F-actin inside the cytoplasm, green), and DAPI (for nucleus, blue). Scale bars are 50 μm.

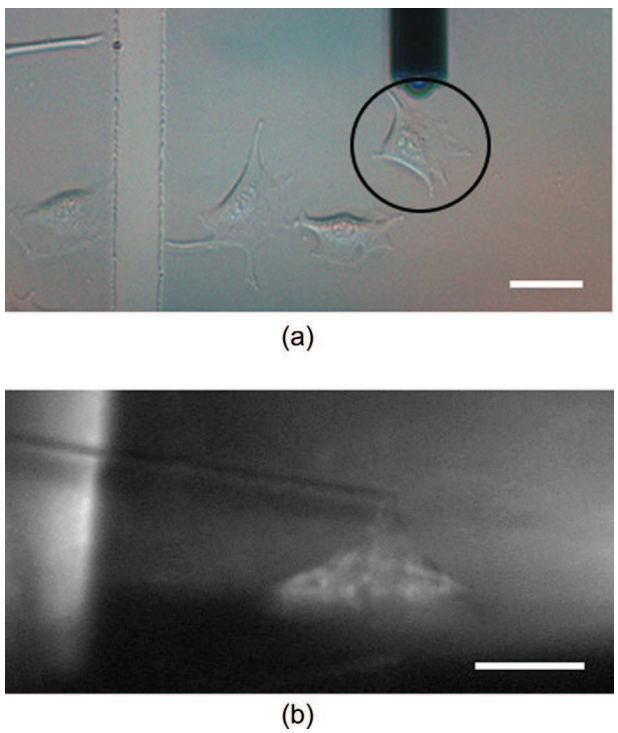

FIG. 4. (a) Top view of the pickup process. The image was taken before the cell adhesion measurement; the circle indicates the cell targeted by the FluidFM cantilever. (b) Side view of the pickup process, using fluorescently tagged C2C12 cells in front of a miniature prism. The thin, bright line within the cantilever is the microfluidic channel connected to the pressure controller of the FluidFM setup. The scale bars are 50 μm.

prism to access the side view, as well as references to the corresponding movies.

Force–distance curves of single-cell detachment provide direct and detailed access to cell adhesion properties. Figure 5 shows representative curves in control condition and after applying a current dose of 12.3 As/m^2, depicting the characteristic properties of maximum adhesion force (detachment force), total distance of detachment (detachment distance), and total work of detachment (detachment work). The dashed curves correspond to the fitted predictions of a simple elastic model; see supplementary material S3 for the details of the model. Based on the model, the slope of the initial, linear part of the force–distance curves is proportional to the Young's modulus of the cells. This slope of the fitted curves, further called static elastic fit parameter, was used to characterize the elastic properties of the cells. The bar plots of Fig. 6 summarize the changes as functions of the applied current dose. In control conditions, the measured maximum cell adhesion force was found to be 520 nN $\pm$ 13%, while the elastic fit given by the model corresponds to a Young's modulus of 2.2 kPa $\pm$ 22%, when using values typical for the C2C12 cell geometry in control conditions. Both the measured maximum cell adhesion force and the calculated value of the Young's modulus are in good agreement with typical values found in the literature. Peeters *et al*. has been estimated the elastic modulus of C2C12 cells to be 2.12 $\pm$ 0.9 kPa,[50] while Potthof *et al*. measured 473 $\pm$ 127 nN maximum adhesion force for HeLa cells cultured on glass.[35] Following the plot of Fig. 6(a),

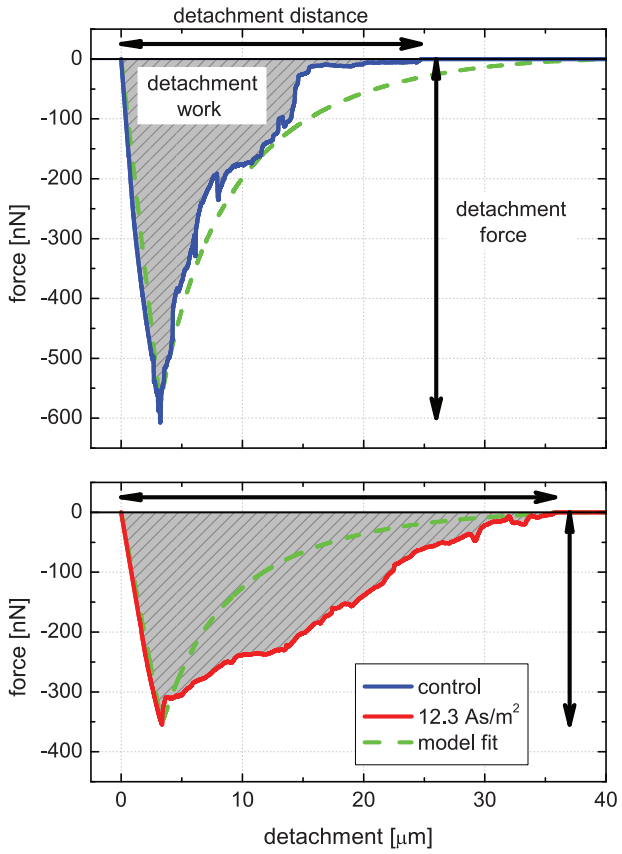

FIG. 5. Representative examples of the force–distance curves in control conditions and after applying a current dose of 12.3 As/m^2. Detachment force is defined by the maximum force needed to detach the cell, and detachment distance is the vertical distance the cantilever was retracted until the cell was completely detached from the substrate, while detachment work was calculated as the integral of the force–distance curve. Dashed curves correspond to the results of model calculations described in the text and in more details in supplementary material S3.

current doses smaller than 11 As/m^2 resulted only in a small, nonsignificant increase in the maximum cell adhesion force. Stimulated with current doses in the range of 11–16 As/m^2, cells with the rounded shape seen in the morphology study could be associated with slightly smaller adhesion forces compared to that of the control cells, while at current doses higher than 16 As/m^2, the maximum adhesion force became significantly higher, presumably as a sign of "frying" the cells on(to) the electrode by destroying the various cellular structures via the electropolymerization of biomolecules. Results from the elastic fit and total detachment work depicted in Figs. 6(b) and 6(d) show similar trends but more pronounced differences in the current dose range of 6–11 As/m^2, supported also by the analysis of the total distance of detachment presented in Fig. 6(c). All these properties showed increased values compared to the control in this range, while no clear changes in viability or maximum adhesion force were detected. The decrease in the extracellular *p*H due to the applied current could be responsible for the effect,[23,51] but the positively charged current electrode itself may also result in changes related to cell adhesion according to the work of McNamee *et al.*, which showed that positively charged particles give strong adhesive forces with melanoma cells.[52] The increase is probably related to the different composition/orientation of extracellular matrix proteins on differently polarized surfaces; however, the exact mechanism is not yet clear at this stage. At higher current doses the detachment distance increased further, sometimes even exceeding the maximum cantilever retraction length possible with the present setup. If moving the cantilever parallel to the substrate in these cases, cells could sometimes be stretched as long as a few hundreds of microns away from the attachment site. See supplementary movie M6 for an example. Focusing more on the 11–16 As/m^2 current dose range, since the static elastic properties here do not show significant differences compared to the control, the reason for significantly longer detachment distances should originate from other, presumably dynamic properties. Alterations in the dynamics of actin reorganization, as a consequence of the increased calcium concentration[2] resulting also in smaller adhesion forces,[53] could be an explanation for such an effect. The possible importance of the change in the dynamic nature of the underlying processes is further emphasized by the measured and calculated force–distance curves of Fig. 5. Whereas the simple model assuming steady state detachment steps fits the control curve rather well and slightly overestimates the real force values during the whole detachment process, it remarkably underestimates the values of the force–distance curve measured after applying a current dose of 12.3 As/m^2, suggesting a much slower, damped dynamics in this case. Differences in actin reorganization are also related to cell death, both apoptotic and necrotic, and while cells lacking vinculin are less stiff than normal cells,[54] both increase and decrease in stiffness has been reported in the literature.[55] This might also explain the increased values of the mean as well as the error bar of the elastic properties representing the >16 As/m^2 current dose range in Fig. 6(b). The "fixing" of the cells on the electrodes indicated by the high detachment force values in this range naturally leads to maximal detachment distances and total detachment work values as well, while live/dead staining still shows these cells viable up to the lethal current dose of 20 As/m^2.

IV. CONCLUSIONS

The importance of electrical stimulus is often underrated in tissue engineering, although it might offer an easy and cost-effective method to regulate cell function in future *in vitro* and *in vivo* applications. Electrical stimulation, for example, can affect cell alignment, and thus, provide more control in tissue engineering for better mimicking tissues found *in vivo*.[6,16] Here, we studied how adhesive and mechanical properties of adherent cells can be manipulated by the use of electric currents. The effect has been quantified in terms of cell morphology, viability, changes in the cytoskeleton and focal adhesion, as well as single-cell force spectroscopy based on the FluidFM technology.

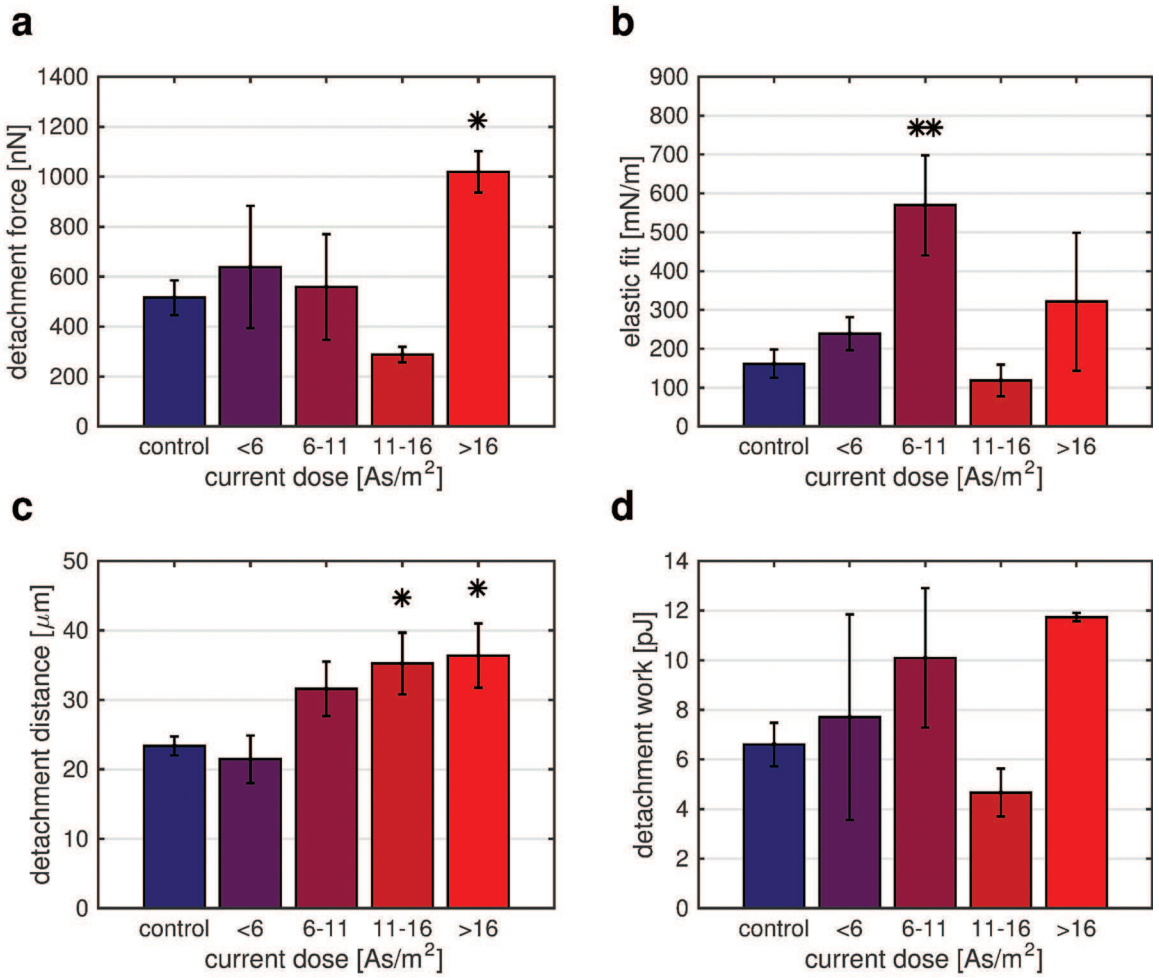

FIG. 6. Detachment force (a), elastic fit [(b), see the text for details], detachment distance (c), and detachment work (d) at different current doses. Data are presented as mean ± the standard error, while single and double asterisks indicate $p < 0.05$ and $p < 0.01$ significance levels as compared to the control, respectively.

While the cell spreading area decreased monotonously with increasing current doses, small current doses below 11 As/m^2 resulted only in differences related to cell elasticity, showing an over 3.5-fold increase of the calculated Young's modulus in the current dose range of 6–11 As/m^2 compared to that of the control. More drastic changes started to happen in the 11–16 As/m^2 current dose range. With a significant drop in viability, the live cell population shrank to approximately 50% of the control both in viability and cell area, the cell morphology started to become more rounded, the cellular structure showed less clear actin fibers and vinculin structures, all accompanied by a decreased adhesion strength and elastic properties. The results of model calculations suggest that alterations in the dynamic nature of actin reorganization might be responsible for these changes resulting in slower, damped dynamics, in agreement with the significantly longer detachment distances found in the corresponding current dose range as compared to the control. At even higher current doses, cell morphology became circular and the vinculin structures had disassembled; however, the adhesion strength significantly increased, presumably due to a radical actin reorganization that also resulted in cell death. After stimulated with current doses above 20 As/m^2, all the cells appeared circular and dead, with the cell area shrinking below 40% of the control. The observed differences in viability starting at current doses above 11 As/m^2 and eventually leading to cell death toward higher doses might originate from both the decrease in *p*H and the generation of ROS. At high current doses, lower current densities for longer times were proved to be more lethal than higher current densities for shorter times, possibly due to the accumulation of these species. Even though high levels are toxic for the cells, physiological amounts of ROS have a positive effect for example on stem cell survival, and also regulate their fate decisions.[56] In a similar study, electrical stimulation could provide a controlled, well-defined method to release ROS for stem cells and find thresholds and optimal conditions for the different cellular behaviors. Stem cells and differentiated cells are also known to have distinct mechanical properties, and thus, modifying their elastic modulus with localized electric stimuli could offer a tool to initiate and enhance their differentiation processes on the single-cell level.[57]

ACKNOWLEDGMENTS

This work was supported by the Finnish Cultural Foundation, the Swiss National Science Foundation, and the 3DNeuroN Project in the European Unions Seventh Framework Program, Future and Emerging Technologies, Grant Agreement No. 296590. The authors thank Stephen Wheeler (ETHZ, LBB) for his valuable technical support, and acknowledge the Laboratory for Urologic Tissue Engineering and Stem Cell Therapy at the University Hospital Zurich for providing access to the fluorescent microscope used for the focal adhesion imaging, as well as Luca Hirt (ETHZ, LBB) for the idea of using the prism to take the side view images.

[1]P. A. Janmey and C. A. McCulloch, Annu. Rev. Biomed. Eng. **9**, 1 (2007).
[2]I. Titushkin and M. Cho, Biophys. J. **96**, 717 (2009).
[3]B. Pontes *et al*., PLoS One **8**, e67708 (2013).
[4]S. Sun, I. Titushkin, and M. Cho, Bioelectrochemistry **69**, 133 (2006).
[5]C. D. McCaig, A. M. Rajnicek, B. Song, and M. Zhao, Physiol. Rev. **85**, 943 (2005).
[6]R. Balint, N. Cassidy, and S. Cartmell, Tissue Eng., Part B **19**, 48 (2013).
[7]M. R. Cho, H. S. Thatte, M. T. Silvia, and D. E. Golan, Faseb J. **13**, 677 (1999).
[8]I. A. Titushkin, V. S. Rao, and M. R. Cho, IEEE Trans. Plasma Sci. **32**, 1614 (2004).
[9]M. R. Cho, H. S. Thatte, R. C. Lee, and D. E. Golan, Faseb J. **8**, 771 (1994).
[10]M. Zhao, A. Dick, J. V. Forrester, and C. D. McCaig, Mol. Biol. Cell **10**, 1259 (1999).
[11]P.-H. Grace Chao, H. H. Lu, C. T. Hung, S. B. Nicoll, and J. C. Bulinski, Connect. Tissue Res. **48**, 188 (2007).
[12]A. L. Berrier and K. M. Yamada, J. Cell. Physiol. **213**, 565 (2007).
[13]M. Benoit, D. Gabriel, G. Gerisch, and H. E. Gaub, Nat. Cell Biol. **2**, 313 (2000).
[14]M. D. Sjaastad, R. S. Lewis, and W. J. Nelson, Mol. Biol. Cell **7**, 1025 (1996).
[15]A. M. Rajnicek, "Neuronal growth cone guidance by physiological DC electric fields," in *The Physiology of Bioelectricity in Development, Tissue Regeneration, and Cancer*, edited by C. E. Pullar (CRC, Boca Raton, FL, 2011), Chap. 10, pp. 201–231.
[16]C. D. McCaig, B. Song, and A. M. Rajnicek, J. Cell Sci. **122**, 4267 (2009).
[17]N. C. Blumenthal, J. Ricci, L. Breger, A. Zychlinsky, H. Solomon, G. G. Chen, D. Kuznetsov, and R. Dorfman, Bioelectromagnetics **18**, 264 (1997).
[18]C. R. Keese, J. Wegener, S. R. Walker, and I. Giaever, Proc. Natl. Acad. Sci. U. S. A. **101**, 1554 (2004).
[19]F. Hofmann, H. Ohnimus, C. Scheller, W. Strupp, U. Zimmermann, and C. Jassoy, J. Membr. Biol. **169**, 103 (1999).
[20]M. Ozkan, T. Pisanic, J. Scheel, C. Barlow, S. Esener, and S. N. Bhatia, Langmuir **19**, 1532 (2003).
[21]O. Guillaume-Gentil, M. Gabi, M. Zenobi-Wong, and J. Vörös, Biomed. Microdevices **13**, 221 (2011).
[22]C. Stock, B. Gassner, C. R. Hauck, H. Arnold, S. Mally, J. A. Eble, P. Dieterich, and A. Schwab, J. Physiol. **567**, 225 (2005).
[23]J. Tan, R. A. Gemeinhart, M. Ma, and W. Mark Saltzman, Biomaterials **26**, 3663 (2005).
[24]K. G. Beaumont and M. Mrksich, Chem. Biol. **19**, 711 (2012).
[25]K. V. Christ and K. T. Turner, J. Adhes. Sci. Technol. **24**, 2027 (2010).
[26]A. Khalili and M. Ahmad, Int. J. Mol. Sci. **16**, 18149 (2015).
[27]A. V. Taubenberger, D. W. Hutmacher, and D. J. Muller, Tissue Eng., Part B **20**, 40 (2014).
[28]R. M. Hochmuth, J. Biomech. **33**, 15 (2000).
[29]N. Walter, C. Selhuber, H. Kessler, and J. P. Spatz, Nano Lett. **6**, 398 (2006).
[30]M. Andersson *et al*., Rev. Sci. Instrum. **78**, 074302 (2007).
[31]M. Benoit and H. E. Gaub, Cells Tissues Organs **172**, 174 (2002).
[32]G. Weder, J. Vörös, M. Giazzon, N. Matthey, H. Heinzelmann, and M. Liley, Biointerphases **4**, 27 (2009).
[33]G. Weder, O. Guillaume-Gentil, N. Matthey, F. Montagne, H. Heinzelmann, J. Vörös, and M. Liley, Biomaterials **31**, 6436 (2010).
[34]A. Meister *et al*., Nano Lett. **9**, 2501 (2009).
[35]E. Potthoff, O. Guillaume-Gentil, D. Ossola, J. Polesel-Maris, S. LeibundGut-Landmann, T. Zambelli, and J. A. Vorholt, PloS One **7**, e52712 (2012).
[36]P. Dörig, P. Stiefel, P. Behr, E. Sarajlic, D. Bijl, M. Gabi, J. Vörös, J. A. Vorholt, and T. Zambelli, Appl. Phys. Lett. **97**, 023701 (2010).
[37]M. Gabi, T. Sannomiya, A. Larmagnac, M. Puttaswamy, and J. Vörös, Integr. Biol. **1**, 108 (2009).
[38]M. Gabi, A. Larmagnac, P. Schulte, and J. Vörös, Colloids Surf. B **79**, 365 (2010).
[39]See supplementary material at http://dx.doi.org/10.1116/1.4940214 for the different chamber and electrode configurations (S1), descriptions of the supplementary movies (S2), as well as details of the elastic model used for the calculations (S3).
[40]J. E. Sader, J. W. M. Chon, and P. Mulvaney, Rev. Sci. Instrum. **70**, 3967 (1999).
[41]G. H. Lee, J. D. Hwang, J. Y. Choi, H. J. Park, J. Y. Cho, K. W. Kim, H. J. Chae, and H. R. Kim, Int. J. Biochem. Cell Biol. **43**, 1305 (2011).
[42]H. Sauer, G. Rahimi, J. Hescheler, and M. Wartenberg, J. Cell. Biochem. **75**, 710 (1999).
[43]E. Serena, E. Figallo, N. Tandon, C. Cannizzaro, S. Gerecht, N. Elvassore, and G. Vunjak-Novakovic, Exp. Cell Res. **315**, 3611 (2009).
[44]P. Chiarugi *et al*., J. Cell Biol. **161**, 933 (2003).
[45]Y. Huo, W.-Y. Qiu, Q. Pan, Y.-F. Yao, K. Xing, and M. F. Lou, Exp. Eye Res. **89**, 876 (2009).
[46]K. M. Connor *et al*., Cancer Res. **67**, 10260 (2007).
[47]H.-U. Simon, A. Haj-Yehia, and F. Levi-Schaffer, Apoptosis **5**, 415 (2000).
[48]N. D. Gallant, K. E. Michael, and A. J. Garcia, Mol. Biol. Cell **16**, 4329 (2005).
[49]C. Gonnermann, C. Huang, S. F. Becker, D. R. Stamov, D. Wedlich, J. Kashef, and C. M. Franz, Integr. Biol. **7**, 356 (2015).
[50]E. A. G. Peeters, C. W. J. Oomens, C. V. C. Bouten, D. L. Bader, and F. P. T. Baaijens, J. Biomech. Eng. **127**, 237 (2005).
[51]R. K. Paradise, D. A. Lauffenburger, and K. J. Van Vliet, PloS One **6**, e15746 (2011).
[52]C. E. McNamee, N. Pyo, and K. Higashitani, Biophys. J. **91**, 1960 (2006).
[53]B. Alberts, A. Johnson, J. Lewis, M. Raff, K. Roberts, and P. Walter, *Molecular Biology of the Cell*, edited by B. Alberts, 5th ed. (Garland Science, New York, 2007), Vol. 16, p. 1503.
[54]F. J. Alenghat, B. Fabry, K. Y. Tsai, W. H. Goldmann, and D. E. Ingber, Biochem. Biophys. Res. Commun. **277**, 93 (2000).
[55]N. I. Nikolaev, T. Müller, D. J. Williams, and Y. Liu, J. Biomech. **47**, 625 (2014).
[56]S. Sart, L. Song, and Y. Li, Oxid. Med. Cell. Longevity **2015**, 1.
[57]D. A. Lee, M. M. Knight, J. J. Campbell, and D. L. Bader, J. Cell. Biochem. **112**, 1 (2011).